

A magnetic reconnection origin for the soft X-ray excess in AGN

Xiaogu Zhong^{1,2,3}, Jiancheng Wang^{1,2}

guqian29@ynao.ac.cn

ABSTRACT

We present a new scenario to explain the soft X-ray excess in Active Galactic Nucleus. The magnetic reconnection could happen in a thin layer on the surface of accretion disk. Electrons are accelerated by shock wave and turbulence triggered by magnetic reconnection, then they take place inverse Compton scattering above accretion disk which contributes soft X-rays. Based on standard disk model, we estimate the magnetic field strength and the energy released by magnetic reconnection along accretion disk, and find that the luminosity caused by magnetic reconnection mainly emits in the inner disk which is dominated by radiation pressure. We then apply the model to fit the spectra of AGNs with strong soft X-ray excess.

Subject headings: galaxies: active - accretion, accretion disks - galaxies: magnetic fields - X-rays: galaxies

1. Introduction

The soft X-ray excess is a major component of many type 1 active galactic nuclei (AGN), especially Narrow Line Seyfert 1 (NLS1) galaxies (e.g. Boller et al. 1996; Laor et al. 1997). Below 1 keV in the X-ray band, the X-ray data are above the low energy extrapolation of the best fitting 2-10 keV power law by index about $\Gamma \sim 2.0$ (Gondhalekar et al. 1997), this is so-called soft X-ray excess. Historically, the soft X-ray excess has often been fitted using a black body model, yielding best-fit temperatures in the range of 0.1-0.2 keV (Czerny et al. 2003; Gierliski & Done 2004). Standard disk model (Shakura & Sunyaev 1973) gives a maximum

¹National Astronomical Observatories, Yunnan Observatory, Chinese Academy of Sciences, Kunming 650011, China

²Key Laboratory for the Structure and Evolution of Celestial Objects, Chinese Academy of Sciences, Kunming 650011, China

³Graduate School, Chinese Academy of Sciences, Beijing, P.R. China

effective temperature of the accreting material of $kT \sim 10(\frac{\dot{m}}{m_s})^{1/4} \text{eV}$, where \dot{m} is the accretion rate in unit of Eddington accretion rate (e.g. $\dot{m} = \dot{M}/\dot{M}_E$) and $m_s = M/10^8 M_\odot$. However, according to this model, only with high accretion rate and low-mass black holes, the peak of accretion disk blackbody spectrum is just at 0.1 keV . But the current observation shows that the black hole mass of source with soft X-ray excess exceeds $10^6 M_\odot$ (Crummy et al. 2006). Because different NLS1 have different mass and accretion rate, the blackbody spectrum of accretion disk is difficult to maintain a stable temperature within the range of $0.1\text{-}0.2 \text{ keV}$. Standard disc model is difficult to explain these properties (Turner & Pounds 1989; Done et al. 2012).

From the analysis of the soft X-ray data, it is found that strong emission and absorption features appear in the soft X-ray spectra of most AGN. As discussed by Gierliski & Done (2004), the imprint of spectral features such as the strong jump in opacity at $\sim 0.7 \text{ keV}$ from O_{VII} , O_{VIII} and Fe M-Shell can lead to an apparent soft excess below this energy. However, the problem is that some parts of the soft excess is often smooth, and certain predicted features are not evident. Schurch & Done (2007, 2008) computed the X-ray spectra of outflow gas with density and velocity, demonstrating that high outflow velocity would be required if absorption in outflows solely explain soft excesses observed in AGN spectra. The high velocity with $0.9 c$ even exceeds the relativistic wind components detected through energy shifted absorption lines, and Schurch et al. (2009) have found that the models of line-driven accretion-disk winds do not attain sufficiently high velocities.

The origin of the soft X-ray excess in AGNs is as yet unknown, we try to explore new radiation mechanism through considering the roles of the magnetic field in accretion disks. We present a new scenario follow as: the magnetic reconnection could happen in a thin layer on the surface of accretion disk like solar active region (Kurtz 1984). Electrons are accelerated by shock wave and turbulence triggered by magnetic reconnection (Kirk et al. 1994), then these electrons emit the X-rays through Compton scattering the photons from the accretion disk. In Section 2, we estimate the magnetic field and the energy released by magnetic reconnection on accretion disks to show whether the released magnetic energy can provide the radiation of soft X-ray excess. In Section 3, we depict the radiative processes and obtain the Compton spectrum. In Section 4, we apply new model to AGNs with strong soft X-ray excess. Finally, Section 5 summarizes our main results and presents our conclusions.

2. Magnetic Field And Energy Release

We assume that the magnetic reconnection emerges frequently in a thin-layer on the surface of standard accretion disk. In the past works, the calculation of the magnetic

field B adopts the equipartition of gas energy and magnetic energy in the disk given by Miller & Stone (2000), $\xi \equiv n_{disk}kT_{disk}/(B^2/8\pi)$, but this result is not a useful guide because they ignore radiation and assume isothermal equation of state, and don't give how the magnetic field scales in the radiation dominated regime. In fact, it is unclear why the magnetic energy density should scale as a constant fixed ratio of the midplane gas pressure. The best numerical simulations have been done by Hirose et al. (2009a,b) and Blaes et al. (2011). Their simulations show that the vertically averaged rms of the magnetic field scales as the square root of the total (gas + radiation) pressure, e.g.

$$B = \sqrt{8\pi\xi^{-1}(nkT + \frac{aT^4}{3})}, \quad (1)$$

where $a = 7.564 \times 10^{-15} \text{erg} \cdot \text{cm}^{-3} \text{K}^{-4}$. Fig. 1 show the distribution of the magnetic field against the radius of accretion disc in unit of R_S with the parameters of $\alpha = 0.1$, $\xi = 1$ and $10^8 M_\odot$. It is shown that the magnetic field rapidly declines along the radius of the accretion disk inside about $20R_S$, but is relatively flat outside $20R_S$, in which the different curves are calculated at the accretion rates \dot{m} of 0.01, 0.1 and 1 respectively (\dot{m} is in the unit of Eddington accretion rate). The magnetic field in the inner disk is stronger than that in the outer disk, implying that the magnetic energy is mainly deposited in the inner disk. We calculate the energy released by fast magnetic reconnection on the accretion disk, in which the magnetic dissipation scales as B^2V_A , and V_A is the Alfvén speed. But it has an upper limit near the disk surface, which is limited by the Poynting flux (see Fig.2) as (Hirose et al. 2006):

$$F_p = fc_s \frac{B^2}{8\pi}, \quad (2)$$

where the factor f represents the departure from hydrostatic balance which permits the upward motion, and c_s is the sound velocity. From Fig.2, we know that the Poynting flux rapidly decreases from the innermost steady radius to $20R_S$. Because the gas pressure is far less than the radiation pressure inside $20R_S$, the Poynting flux is approximately given by:

$$F_p \approx 4.98 \times 10^{18} \left(\frac{4}{3} + \frac{2}{\xi}\right)^{\frac{1}{2}} \alpha^{-1} m_8^{-1} \dot{m} \left(\frac{R}{R_S}\right)^{-3} f \xi^{-1} \text{erg} \cdot \text{cm}^{-2} \text{s}^{-1}, \quad (3)$$

where R_S is the Schwarzschild radius. Assuming almost all energy released by magnetic reconnection be converted to soft X-ray radiation energy, we can estimate the maximum of soft X-ray luminosity by integrating the Poynting flux from the inner radius to $20R_S$ as:

$$L_{soft} \approx 2.81 \times 10^{46} \left(\frac{4}{3} + \frac{2}{\xi}\right)^{\frac{1}{2}} \alpha^{-1} m_8^2 \dot{m} f \xi^{-1} \text{erg} \cdot \text{s}^{-1}. \quad (4)$$

3. The Radiative Processes

3.1. The electron spectrum

Considering that electrons are accelerated by shock wave and turbulence in magnetic reconnection, we can obtain the electron energy spectrum as (Droege & Schlickeiser 1986):

$$F(E) = AE^{-q(E)}, \quad (5)$$

where the electron spectrum index is

$$q(E) = -\frac{\eta + a + 1}{2} + \frac{3 + a - \eta}{2} \left[1 + \frac{4\lambda\sqrt{2m_e}^{\eta+b}}{(3 + a - \eta)^2} E^{(\eta+b)/2} \right]^{1/2}, \quad (6)$$

and the parameters η , a , λ and b are determined by the microcosmic structure of the shock wave and turbulence expressed as follows (Bogdan & Schlickeiser 1985; Droege & Schlickeiser 1986):

$$\begin{aligned} T(p) &= T_0 p^{-b}, \\ K(p) &= \delta v(p) p^{2-q} = \kappa p^\eta, \\ D(p) &= \alpha_2 \frac{V_A^2}{K} p^2, \\ \dot{p}_G &\approx \alpha_1 \frac{V_S^2}{K} p^2, \end{aligned}$$

where $a = \alpha_1 V_S^2 / \alpha_2 V_A^2$, $\lambda = \kappa / \alpha_2 V_A^2 T_0$. When the electrons are not accelerated to high energy for fast magnetic reconnection, the electron spectrum will become a power-law with constant index (Droege & Schlickeiser 1986), given by

$$F(E) = AE^{-q}, E_1 \leq E \leq E_2; \quad (7)$$

E_1 and E_2 are the cutoffs in the spectrum. When $E_2 \gg E_1$ and $q > 1$, the factor A is given by $A = N_e(q - 1)E_1^{q-1}$, in which N_e is the number density of electrons. The kinetic energy E of non-relativistic electron is expressed as $E = (\gamma - 1)m_e c^2$, in which $\gamma = 1/\sqrt{1 - \beta^2}$ and βc are the Lorentz factor and velocity of the electron. When $E \ll m_e c^2$, $\beta = \sqrt{2E/m_e c^2}$.

3.2. Comparison of electron energy losses through Bremsstrahlung and Compton radiation

The electron in magnetic field will take place bremsstrahlung, inverse Compton scattering and synchrotron emission. Because the electron is non-relativistic, we can ignore synchrotron radiation. Next, we will compare the electron energy losses through bremsstrahlung and Compton radiation.

The energy loss rate of the electron with the energy E in Compton radiation is given by (Blumenthal & Gould 1970)

$$\frac{dE}{dt} = \sigma_T c \gamma^2 \int (1 - \beta \cos \theta)^2 \epsilon dn = \sigma_T c \gamma^2 (1 + \frac{1}{3} \beta^2) U_{ph}, \quad (8)$$

where σ_T is the Thompson cross section, U_{ph} is the energy density of soft photons. The total energy loss rate of the non-thermal electrons is given by

$$\begin{aligned} P_c &= \sigma_T c U_{ph} \int_{E_1}^{E_2} A \gamma^2 (1 + \frac{1}{3} \beta^2) E^{-q} dE, \\ &= \sigma_T c U_{ph} N (q - 1) \left(\frac{E_1}{m_e c^2} \right)^{q-1} \int_{\beta_1}^{\beta_2} \gamma^5 \beta (1 + \frac{1}{3} \beta^2) (\gamma - 1)^{-q} d\beta. \end{aligned} \quad (9)$$

The energy loss rate of the electron with the energy E in Bremsstrahlung radiation is given by (Gould 1980)

$$\frac{dE}{dt} = \frac{2}{\pi} \sigma_T n_Z Z^2 \alpha_f m_e c^3 \beta (1 + \frac{5}{12} \beta^2), \quad (10)$$

$\alpha_f = \frac{1}{137}$ is the fine structure constant, n_Z is the number density of the ion. The total energy loss rate is

$$\begin{aligned} P_b &= \sum_Z n_Z Z^2 \frac{2}{\pi} \sigma_T \alpha_f m_e c^3 A \int_{E_1}^{E_2} \beta (1 + \frac{5}{12} \beta^2) E^{-q} dE, \\ &= \sum_Z n_Z Z^2 \frac{2}{\pi} \sigma_T \alpha_f m_e c^3 N (q - 1) \left(\frac{E_1}{m_e c^2} \right)^{q-1} \int_{\beta_1}^{\beta_2} \gamma^3 \beta^2 (1 + \frac{5}{12} \beta^2) (\gamma - 1)^{-q} d\beta. \end{aligned} \quad (11)$$

Then we have

$$\frac{P_c}{P_b} = \frac{\pi U_{ph}}{2 \alpha_f n_p m_e c^2} \frac{H_1(\beta_1, \beta_2)}{H_2(\beta_1, \beta_2)}, \quad (12)$$

where $n_p = \sum n_Z Z^2$,

$$H_1(\beta_1, \beta_2) = \int_{\beta_1}^{\beta_2} \gamma^5 \beta (1 + \frac{1}{3} \beta^2) (\gamma - 1)^{-q} d\beta, \quad (13)$$

and

$$H_2(\beta_1, \beta_2) = \int_{\beta_1}^{\beta_2} \gamma^3 \beta^2 (1 + \frac{5}{12} \beta^2) (\gamma - 1)^{-q} d\beta. \quad (14)$$

In the accretion disk, $U_{ph} = \sigma T_{eff}^4/c$, T_{eff} is the effective temperature of disk, σ is the radiation constant, and n_p takes the number density of the proton, we obtain

$$\frac{P_c}{P_b} = \frac{\pi\sigma T_{eff}^4}{2\alpha_f n_p m_e c^3} \frac{H_1(\beta_1, \beta_2)}{H_2(\beta_1, \beta_2)} = 1.78 \times 10^7 \alpha \dot{m}^3 r^{-\frac{9}{2}} (1 - r^{-\frac{1}{2}})^2 \frac{H_1(\beta_1, \beta_2)}{H_2(\beta_1, \beta_2)}, \quad (15)$$

where $r = R/3R_s$, $\dot{m} = \dot{M}/\dot{M}_{Edd}$, and \dot{M}_{Edd} is the Eddington accretion rate. Because $H_1(\beta_1, \beta_2) > H_2(\beta_1, \beta_2)$, $P_c \gg P_b$ in the inner region of accretion disk for larger accretion rate, indicating that the Compton radiation of electrons dominates the bremsstrahlung radiation.

3.3. Compton radiation

Because the magnetic field decreases along the radius of accretion disk, the parameters of accelerated electrons will change with the radius. Assuming that E_1 , E_2 and q are independent of the magnetic field, we can estimate the number density of electrons along the radius. Assuming that the energy loss rate of electrons equals the magnetic dissipation, e.g., $P_c = \frac{B^2 V_A}{8\pi h_r}$, in which h_r is the characteristic scale of reconnection, we obtain

$$N(R)(q-1)\left(\frac{E_1}{m_e c^2}\right)^{q-1} = \frac{B^2 V_A}{8\pi h_r \sigma_T c U_{ph}} H_1^{-1}(\beta_1, \beta_2). \quad (16)$$

When an electron is not accelerated to a high energy, the Compton spectrum in the Thomson limit given by Blumenthal & Gould (1970) for a relativistic electron should be changed as

$$\frac{dN_{\gamma,\epsilon}}{dt d\epsilon_1} = \frac{\pi r_0^2 c}{2\gamma^4 \beta^4} \frac{n(\epsilon) d\epsilon}{\epsilon^2} \left\{ 2\epsilon_1 \ln \frac{\epsilon_1}{(1+\beta)^2 \gamma^2 \epsilon} + \frac{2\beta}{1+\beta} \epsilon_1 + (1+\beta)(1+\beta^2)\gamma^2 \epsilon - \frac{\epsilon_1^2}{(1+\beta)\gamma^2 \epsilon} \right\}, \quad (17)$$

where $n(\epsilon)d\epsilon$ represents the differential photon density, ϵ_1 expresses the energy of the scattered photon, and the electron has the energy $E = (\gamma - 1)m_e c^2$ and velocity βc . When $\beta \rightarrow 1$, the above formula returns to the Compton spectrum produced by a high energy electron in the Thomson limit (Blumenthal & Gould 1970). It is noted that the above distribution function equals zero at $\beta_* = (\epsilon_1/\epsilon - 1)(\epsilon_1/\epsilon + 1)^{-1}$. Since the differential number of electrons are $dN = AE^{-q}dE$, the total Compton spectrum is given by

$$\frac{dN_\epsilon}{dt d\epsilon_1} = A \int E^{-q} dE \frac{dN_{\gamma,\epsilon}}{dt d\epsilon_1} = N_e(R)(q-1)\left(\frac{E_1}{m_e c^2}\right)^{q-1} \int_{\beta_{min}}^{\beta_{max}} (\gamma-1)^{-q} \gamma^3 \beta d\beta \frac{dN_{\gamma,\epsilon}}{dt d\epsilon_1}, \quad (18)$$

where $d\gamma = \gamma^3 \beta d\beta$, $\beta_{min} = \max[\beta_*, \beta_1]$, $\beta_{max} = \beta_2$, β_1 and β_2 correspond to the energy cutoffs E_1 and E_2 in the electron spectrum. For the soft photons in accretion disk, the

differential photon density $n(\epsilon, R)d\epsilon$ in the radius R is given by

$$n(\epsilon, R)d\epsilon = \frac{8\pi\epsilon^2}{h^3c^3} \left(e^{\frac{\epsilon}{kT(R)}} - 1 \right)^{-1} d\epsilon, \quad (19)$$

where $T(R)$ is the temperature of disk surface in the radius R . We then obtain the Compton spectrum along the radius

$$\begin{aligned} \frac{dN}{dt d\epsilon_1}(R) &= N_e(R)(q-1) \left(\frac{E_1}{m_e c^2} \right)^{q-1} \frac{\pi r_0^2 c}{2} \int_{\epsilon_0}^{\epsilon_1} \frac{n(\epsilon, R)}{\epsilon} H\left(\frac{\epsilon_1}{\epsilon}, q\right) d\epsilon \\ &= \frac{3}{16} \frac{B^2 V_A}{8\pi h_r U_{ph}} H_1^{-1}(\beta_1, \beta_2) \int_{\epsilon_0}^{\epsilon_1} \frac{n(\epsilon, R)}{\epsilon} H\left(\frac{\epsilon_1}{\epsilon}, q\right) d\epsilon, \end{aligned} \quad (20)$$

where

$$H\left(\frac{\epsilon_1}{\epsilon}, q\right) = \int_{\beta_{min}}^{\beta_2} (\gamma-1)^{-q} \gamma^{-1} \beta^{-3} d\beta \zeta\left(\frac{\epsilon_1}{\epsilon}, \beta\right), \quad (21)$$

$$\zeta\left(\frac{\epsilon_1}{\epsilon}, \beta\right) = \frac{\epsilon_1}{\epsilon} \left\{ 2 \ln \frac{\epsilon_1}{\epsilon} \frac{1}{(1+\beta)^2 \gamma^2} + \frac{2\beta}{1+\beta} + \frac{\epsilon}{\epsilon_1} (1+\beta)(1+\beta^2)\gamma^2 - \frac{\epsilon_1}{\epsilon} \frac{1}{(1+\beta)\gamma^2} \right\}, \quad (22)$$

and ϵ_0 is given by $(\epsilon_1/\epsilon_0 - 1)(\epsilon_1/\epsilon_0 + 1)^{-1} = \beta_2$, e.g., $\epsilon_0 = \epsilon_1(1 - \beta_2)/(1 + \beta_2)$. In fact, $H\left(\frac{\epsilon_1}{\epsilon}, q\right)$ can be simplified as

$$\begin{aligned} H\left(\frac{\epsilon_1}{\epsilon}, q\right) &= \int_{\beta_1}^{\beta_2} (\gamma-1)^{-q} \gamma^{-1} \beta^{-3} d\beta \zeta\left(\frac{\epsilon_1}{\epsilon}, \beta\right), \quad 1 \leq \frac{\epsilon_1}{\epsilon} < \frac{1+\beta_1}{1-\beta_1}, \\ H\left(\frac{\epsilon_1}{\epsilon}, q\right) &= \int_{\beta_*}^{\beta_2} (\gamma-1)^{-q} \gamma^{-1} \beta^{-3} d\beta \zeta\left(\frac{\epsilon_1}{\epsilon}, \beta\right), \quad \frac{1+\beta_1}{1-\beta_1} \leq \frac{\epsilon_1}{\epsilon} \leq \frac{1+\beta_2}{1-\beta_2}, \\ H\left(\frac{\epsilon_1}{\epsilon}, q\right) &= 0, \quad \frac{\epsilon_1}{\epsilon} > \frac{1+\beta_2}{1-\beta_2}. \end{aligned} \quad (23)$$

The total Compton radiation spectrum is given by

$$\begin{aligned} L(\epsilon_1) &= \int_{R_{in}}^{R_{out}} 2\pi R h_r \epsilon_1^2 \frac{dN}{dt d\epsilon_1}(R) dR \\ &= \frac{3}{64} H_1^{-1}(\beta_1, \beta_2) \epsilon_1^2 \int_{R_{in}}^{R_{out}} \frac{B^2 V_A}{U_{ph}} \int_{\epsilon_0}^{\epsilon_1} \frac{n(\epsilon, R)}{\epsilon} H\left(\frac{\epsilon_1}{\epsilon}, q\right) d\epsilon R dR, \end{aligned} \quad (24)$$

where we take $R_{in} = 3R_S$ and $R_{out} = 20R_S$ for the radiation-dominated region of accretion disk, and $B^2 V_A / U_{ph}$ is given by

$$\begin{aligned} \frac{B^2 V_A}{U_{ph}} &= \frac{8\pi c}{3\sigma} \xi^{-\frac{3}{2}} \left(\frac{2a^3}{3m_p n_p} \right)^{\frac{1}{2}} \frac{T^6}{T_{eff}^4} \\ &= 3.6 \times 10^9 \alpha^{-1} \xi^{-\frac{3}{2}} (1 - r^{-\frac{1}{2}}) \text{cm.s}^{-1}, \end{aligned} \quad (25)$$

where we use the structure of accretion disk as

$$\begin{aligned} T(R) &= 2.3 \times 10^5 (\alpha m_8)^{-\frac{1}{4}} r^{-\frac{3}{8}} K, \\ n_p(R) &= 4.3 \times 10^9 (\alpha m_8)^{-1} \dot{m}^{-2} r^{\frac{3}{2}} (1 - r^{-\frac{1}{2}})^{-2} \text{cm}^{-3}, \\ T_{eff}(R) &= 6.2 \times 10^5 (\dot{m}^{-1} m_8)^{-\frac{1}{4}} r^{-\frac{3}{4}} K, \end{aligned}$$

and $m_8 = M/10^8 M_\odot$.

Finally we obtain

$$L(\bar{\epsilon}) = 6.9 \times 10^{48} \alpha^{-1} \xi^{-\frac{3}{2}} m_8^2 \bar{L}(\bar{\epsilon}, q, \beta_1, \beta_2) \text{ergs}^{-1}, \quad (26)$$

where $\bar{\epsilon} = \epsilon_1/k\text{eV}$, and

$$\bar{L}(\bar{\epsilon}, q, \beta_1, \beta_2, kT_0) = \bar{\epsilon}^2 H_1^{-1}(\beta_1, \beta_2) \int_1^{r_{out}} (1 - r^{-\frac{1}{2}}) r dr \int_{\bar{\epsilon}_0}^{\bar{\epsilon}} \epsilon \left(e^{\frac{\epsilon}{kT_0} r^{\frac{3}{8}}} - 1 \right)^{-1} H\left(\frac{\bar{\epsilon}}{\epsilon}, q\right) d\epsilon, \quad (27)$$

where $kT_0 = 2.0 \times 10^{-2} (\alpha m_8)^{-\frac{1}{4}}$, which means the temperature of inner stable radius of accretion disk, and $r_{out} = 20/3$, The curves of $\bar{L}(\bar{\epsilon}, q, \beta_1, \beta_2, kT_0)$ with $\bar{\epsilon}$ for the parameters of q, β_1, β_2 and kT_0 are shown in Figure 3-5.

4. Model Application

In this section we apply the model to fit the X-ray spectra (EPIC-pn of XMM-Newton data) of AGNs (PG quasars and NLS1s) with high mass accretion rates given by Crummy et al. (2006) (see Table.1), in which their soft X-ray radiation include thermal radiation and Inverse Compton scattering. The Compton spectrum caused by magnetic reconnection is added in *XSPEC* v12.7.1 (Arnaud 1996) through *initpackage* and *lmod* codes. Due to these samples have different black hole masses and accretion rates, they can get different temperature of the blackbody spectrum of accretion disk. According to the Standard disc model, for high accretion rate and low-mass black holes, the peak of accretion disc blackbody spectrum can arrive at X-ray band and we need to add the blackbody model in spectral fitting. Because the radiation of accretion disk is multi-temperature blackbody spectrum, we use the *diskbb* model of the *XSPEC* to fit thermal spectrum. The powerlaw with spectral index Γ is used to fit the hard X-ray component because the hard X-ray radiation is considered to be from inverse Compton scattering in the accretion disc corona (Liu et al. 2002). For some sources with low black hole mass and high accretion rate, the thermal radiation of accretion disk partly contributes the soft X-rays, we use the mixing model *absorption(diskbb+compton+powerlaw)* to fit soft excess and use the *newpar* code to link kT_0 and the temperature of inner stable

radius of *diskbb*. For other sources with high black hole mass and low accretion rate, the thermal radiation can be ignored due to low blackbody temperature to radiate soft X-rays, we use the mixing model *absorption(compton+powerlaw)* to fit soft excess. In the Compton model, there are four parameters to determine the spectrum, such as kT_0 , q , β_1 and β_2 . The fitting parameters are listed in Table 2, and the fitting spectra are shown in Fig.6-7. Then, we can estimate ξ by equaling the observed soft X-ray luminosity to the Compton luminosity obtained by integrating the equation (26) from $0.1keV$ to $5keV$. Combining the equation (4) that gives the maximum of soft X-ray luminosity, we can estimate the maximum magnetic energy conversion rate, in which we take $f = 0.1$ because the mean growing speed of magnetic structures is $0.1c_s$ (Hirose et al. 2006). The results are listed in Table 3.

5. Discussion and Conclusions

The soft X-ray excess is a major component of the X-ray spectra in many AGNs, and is usually well fitted with a blackbody which has a roughly constant temperature of 0.1-0.2 keV over several decades of AGN mass. If the soft X-rays is thermal, its temperature is too high to be explained by the standard accretion disc model. Although the high temperature can occur in a slim accretion disc (Mineshige et al. 2000), its accretion rate is super-Eddington (Tanaka et al. 2005) and extreme ultraviolet photons are comptonized (Porquet et al. 2004). The strong emission and absorption features are found in the soft X-ray spectra of most AGNs. There is a strong jump in opacity at 0.7 keV from partially ionized material, where OVII/OVIII and Fe M shell unresolved transition array are combined to produce an apparent soft excess which is not intrinsic in two different geometries, either by reflection from optically thick material out of the line of sight, or through absorption by optically thin material in the line of sight. However, both geometries would show characteristic and sharp atomic features which can be smeared by strong relativistic effects in the reflection model, but the parameters required are quite extreme, in which the disc has to extend to the last stable orbit in high spin black hole, and the reflection is highly concentrated in the innermost regions (Crummy et al. 2006). Reflection off the surface of the accretion disc is proposed by Fabian et al. (2002) to explain the soft excess, in which the primary X-rays go through substantial reprocessing in the upper layers of the disc, and emerge as a smooth spectrum due to relativistic blurring. Some sources are explained by disc reflection, such as, Mrk 335 (Larsson et al. 2008), Mrk 478 (Zoghbi et al. 2008), Fairall 9 (Schmoll et al. 2009; Emmanoulopoulos et al. 2011) and Ark 120 (Nardini et al. 2011). A self-consistent, dual-reflector model is needed to explain the soft excess of Ark 120 at the different epochs (Nardini et al. 2012). Recently the intensity-correlated spectral analysis is developed to constrain the origin of the soft X-ray excess in several AGNs (Noda et al.

2011, 2013), in which the Multi-Zone Comptonization is required to interpret a stable soft excess component that is independent of the dominant power-law emission. Mehdipour et al. (2011); Patrice et al. (2013) find that the soft X-ray excess emission varies in association with the UV emission and is independent of the X-ray power-law component based on the UV and X-ray observations of the Mrk 509. A long-look Suzaku observation of the Mrk 509 also support that the soft excess is independent of the X-ray continuum (Rivers et al. 2012). It is indicated that the soft X-ray excess could be produced by the Comptonisation of the thermal optical-UV photons from the accretion disc by a warm corona (Mehdipour et al. 2011) or with the disc photosphere itself (Done et al. 2012). Done et al. (2012) also find that the Compton upscattered soft X-ray excess decreases in importance with increasing L/L_{Edd} , in which the strongest soft excesses are associated with low mass accretion rate AGN rather than being tied to some change in disc structure around Eddington.

Based on the standard disk model, we present a new scenario to explain the soft X-ray excess. The magnetic reconnection is assumed to happen in a thin layer on the surface of accretion disk, its releasing energy accelerates electrons through shock wave and turbulence triggered by itself. These electrons then take place Inverse Compton scattering above accretion disk which contributes soft X-ray excess. We present that the magnetic field declines continuously with the radius of the accretion disk and decreases rapidly in the inside of disk, but is relatively flat in the outside of disk. We then calculate the upper limit of energy released by the Poynting flux on the accretion disk. The distribution of the Poynting flux implies that the soft X-ray excess should emit from the inner region of disk. In the inner region of accretion disk, the gas pressure can be ignored, we estimate the maximum luminosity by integrating the Poynting flux from the innermost steady radius to $20R_S$. In Section.3, we compare the electron energy losses through Bremsstrahlung and Compton radiation. The results show that the electron energy losses through Bremsstrahlung is far less than through Compton radiation. This means that the Compton radiation of electrons dominates the bremsstrahlung radiation. Then, we calculate the Compton spectrum of non-relativistic and non-thermal electrons, and obtain that the Compton spectrum is determined by kT_0 , q , β_1 , β_2 and is independent of accretion rate as found by Winter et al. (2009). From the equation (27), we know that the Compton spectrum is mainly determined by kT_0 . According to the standard disc model, $T_0 \propto M^{-1/4}$ and the masses of black hole in AGN are range of $10^6 M_\odot$ to $10^9 M_\odot$, the Compton spectrum weakly depends on mass. Fig.3 shows that the Compton spectrum with different kT_0 maintain a narrow range of 0.1-0.5 keV corresponding to the characteristic temperature of the soft X-ray excess. Therefore, the Compton spectrum can well fit the soft X-ray excess as shown in Fig.6-7, in which Fig.7 includes the component with multi-temperature blackbody spectrum. It is shown that the soft photons from accretion disk are scattered to higher energy by non-thermal electrons generated by magnetic recon-

nection and contribute the soft excess. We also give the Compton spectrum depending on q , β_1 and β_2 , shown in Fig.4-5. The spectrum keeps similar shape and shifts to low energy with q increasing, while the spectrum also shifts in the energy with β_1 and β_2 . Finally, we estimate the ξ representing magnetic strength and the magnetic energy conversion rate listed in Table 3, and find that the magnetic energy conversion rates are low for many sources.

Acknowledgments

We are grateful to the referee for useful comments improving the paper. We acknowledge the financial supports from the National Basic Research Program of China (973 Program 2009CB824800), the National Natural Science Foundation of China 11133006, 11163006, 11173054, and the Policy Research Program of Chinese Academy of Sciences (KJCX2-YW-T24).

REFERENCES

- Arnaud, K. A. 1996, in Jacoby, G. H., Barnes, J., eds, ASP Conf. Ser Vol. 101, Astronomical Data Analysis Software and Systems V. Astron. Soc.Pac., San Francisco, p. 17
- Blaes, O., Krolik, J. H., Hirose, S., & Shabaltas, N. 2011, ApJ, 733, 110
- Blumenthal, G. R., & Gould, R. J. 1970, Rev. Mod. Phys., 42, 237.
- Bogdan, T. G., & Schlickeiser, R. 1985, A&A, 143, 23
- Boller, T., Brandt, W. N., & Fink, H. 1996, A&A, 305, 53
- Crummy, J., Fabian, A. C., Gallo, L., & Ross, R. R. 2006, MNRAS, 365, 1067
- Czerny, B., Nikolajuk, M., Róžańska, A., Dumont, A. M., Loska, Z., & Zycki, P. T. 2003, A&A, 412, 317
- Done, C., Davis, S. W., Jin, C., Blaes, O., & Ward, M. 2012, MNRAS, 420, 1848
- Droege, W., & Schlickeiser, R. 1986, ApJ, 305, 909
- Emmanoulopoulos, D. et al. 2011, MNRAS, 415, 1895
- Fabian A. C. et al. 2002, MNRAS, 331, L35
- Gierliński, M., & Done, C. 2004, MNRAS, 349, 7

- Gondhalekar, P. M., Rouillon-Foley, C., & Kellett, B. J. 1997, MNRAS, 288, 260
- Gould, R. J. 1980, ApJ, 238, 1026
- Grupe, D., Komossa, S., Leighly, K. M., & Page, K. L. 2010, ApJS, 187, 64
- Hirose, S., Krolik, J. H. & Stone, J. M. 2006, ApJ, 640, 901
- Hirose, S., Blaes, O., & Krolik, J. H. 2009a, ApJ, 704, 781
- Hirose, S., Krolik, J. H., & Blaes, O. 2009b, ApJ, 691, 16
- Kirk, J. G., Melrose, D. B., Priest, E. R., Benz, A. O., & Courvoisier, T. J. L., Plasma Astrophysics, 1994, Springer-Verlag Berlin Heidelberg New York
- Kurtz, D. W. 1984, MNRAS, 43, 22
- Laor, A., Fiore, F., Elvis, M., Wilkes, B. J., & McDowell, J. C. 1997 ApJ, 477, 93
- Larsson, J. et al. 2008, MNRAS, 384, 1316
- Liu, B. F., Mineshige, S., & Shibata, K. 2002, ApJ, 572, 173
- Mahony, E. K., Croom, S. M., Boyle, B. J., et al. 2010, MNRAS, 401, 1151
- Mehdipour, M. et al. 2011, A&A, 534, 39
- Middleton, M., Done, C., & Gierliński, M. 2007, MNRAS, 381, 1426
- Miller, K. A., & Stone, J. M. 2000, ApJ, 534, 398
- Mineshige, S., Kawaguchi, M., & Hayashida, K. 2000, PASJ, 52,499
- Nardini, E., Fabian, A. C., Reis, R. C., & Walton D. J. 2011, MNRAS, 410, 1251
- Nardini, E., Fabian, A. C., & Walton, D. J. 2012, MNRAS, 423,3299
- Noda, H. et al. 2011, PASJ, 63, 925
- Noda, H. et al. 2013, PASJ, 65, 4
- Parker, E. N. 1955, ApJ, 122, 293
- Patrice, P.-O. et al. 2013, A&A, 549, 73
- Piconcelli, E., Jimenez-Bailón, E., Guainazzi, M., et al. 2005, A&A, 432, 15

- Porquet, D., Reeves, J. N., O'Brien, P., & Brinkmann, W., 2004, *A&A*, 422, 85
- Rivers, E. et al. 2012, *ApJ*, 759, 63
- Schmoll, S. et al. 2009, *ApJ*, 703, 2171
- Schurch, N. J., & Done, C. 2007, *MNRAS*, 381, 1413
- Schurch, N. J., & Done, C. 2008, *MNRAS*, 386, 1
- Schurch, N. J., Done, C., & Proga, D. 2009, *ApJ*, 694, 1
- Shakura, N. I., & Sunyaev, R. A. 1973, *A&A*, 24, 337
- Tanaka, Y., Boller, T., & Gallo, L. 2005, in Merloni, A., Nayakshin, S., Sunyaev R., A., eds, *ESO Astrophys. Symp., Growing Black Holes: Accretion in a Cosmological Context*. Springer, Berlin, p. 290
- Tandberg-Hanssen, E., & Emslie, A. G., *The physics of solar flares*, 1988, Cambridge: Cambridge University Press
- Turner, T. J., & Pounds, K. A. 1989, *MNRAS*, 240, 833
- Winter, L. M., Mushotzky, R. F., Reynolds, C. S., & Tueller, J. 2009, *ApJ*, 690, 1322
- Zoghbi, A., Fabian, A. C., & Gallo, L. C. 2008, *MNRAS*, 391, 2003

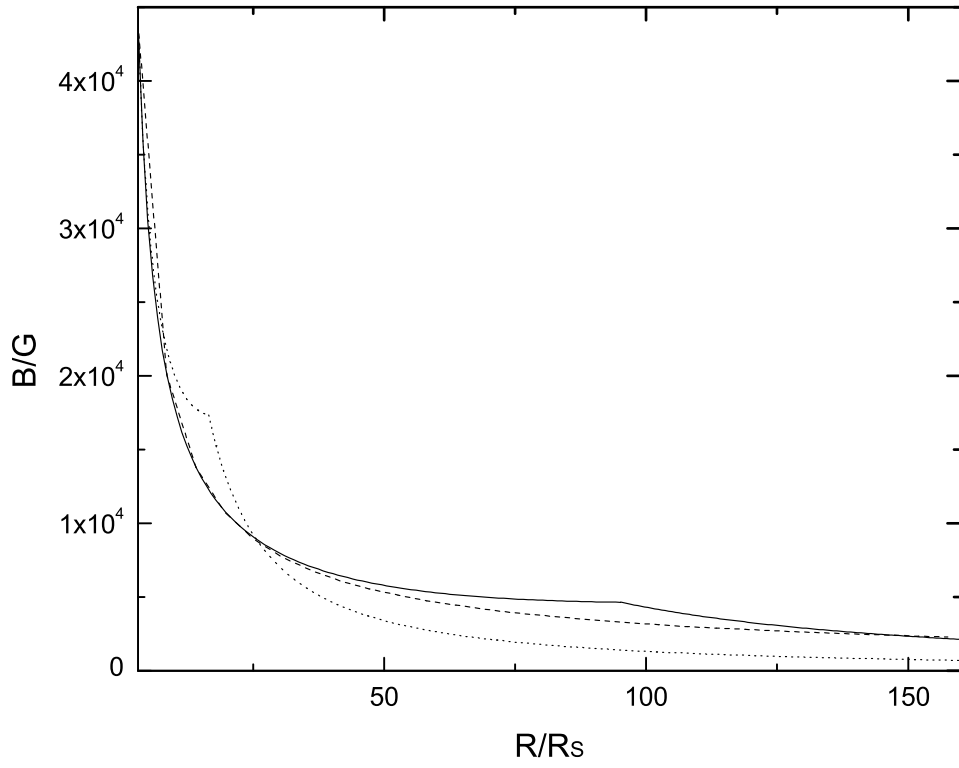


Fig. 1.— The magnetic field against the radius of accretion disc in unit of R_S with $\alpha = 0.1$, $\xi = 1$ and $10^8 M_\odot$. The dash, solid and dot lines correspond to \dot{m} of 1, 0.1 and 0.01 respectively.

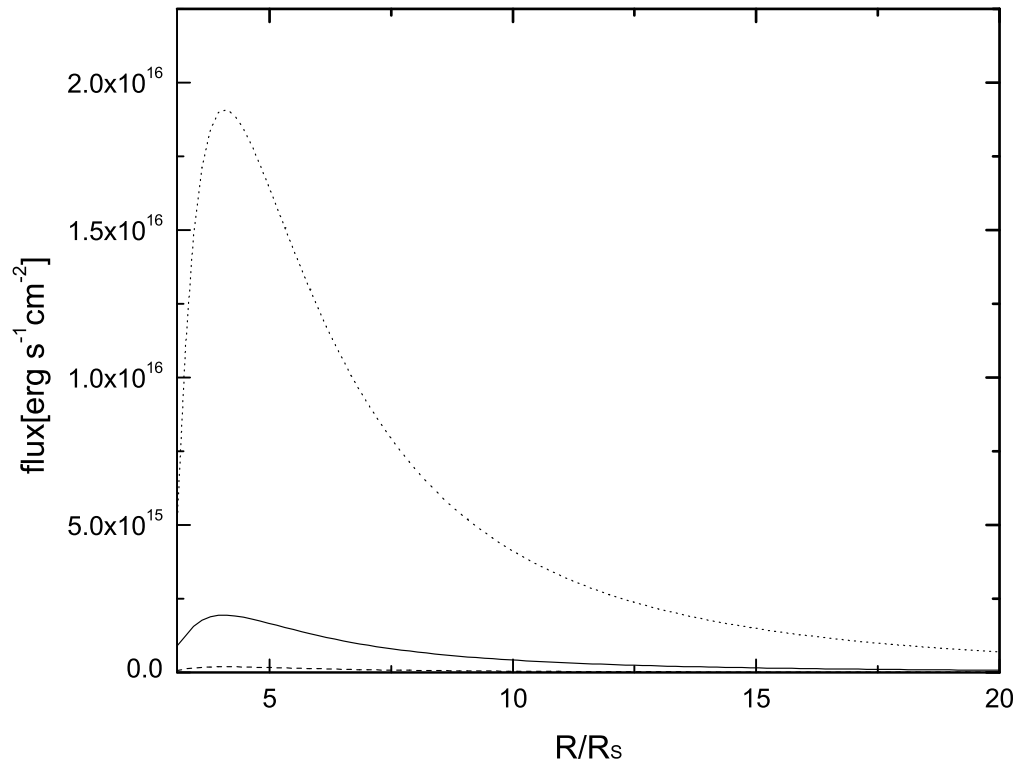


Fig. 2.— The solid and dot lines represent the Poynting flux with $\alpha = 0.1$, $\xi = 1$, $10^8 M_\odot$, $\dot{m} = 0.1$, and $\alpha = 0.1$, $\xi = 1$, $10^8 M_\odot$, $\dot{m} = 1$, respectively. The dash line represent the Poynting flux with $\alpha = 0.1$, $\xi = 1$, $10^9 M_\odot$, $\dot{m} = 0.1$

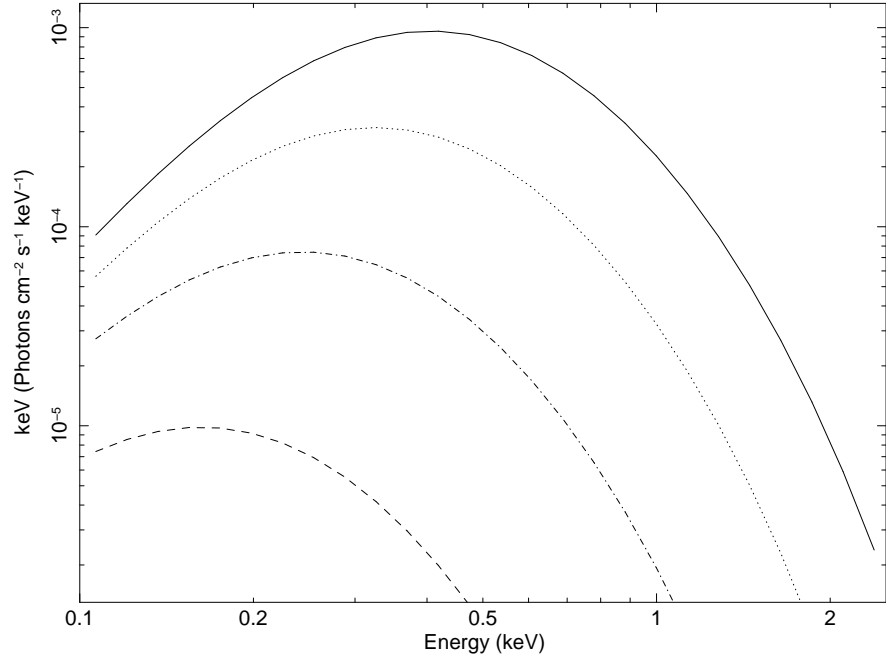


Fig. 3.— The spectral shapes with different kT_0 , in which the dash, dash dot, dotted and solid lines correspond to $kT_0 = 0.04, 0.06, 0.08, 0.1 \text{ keV}$, where $q = 2, \beta_1 = 0.02, \beta_2 = 0.196$

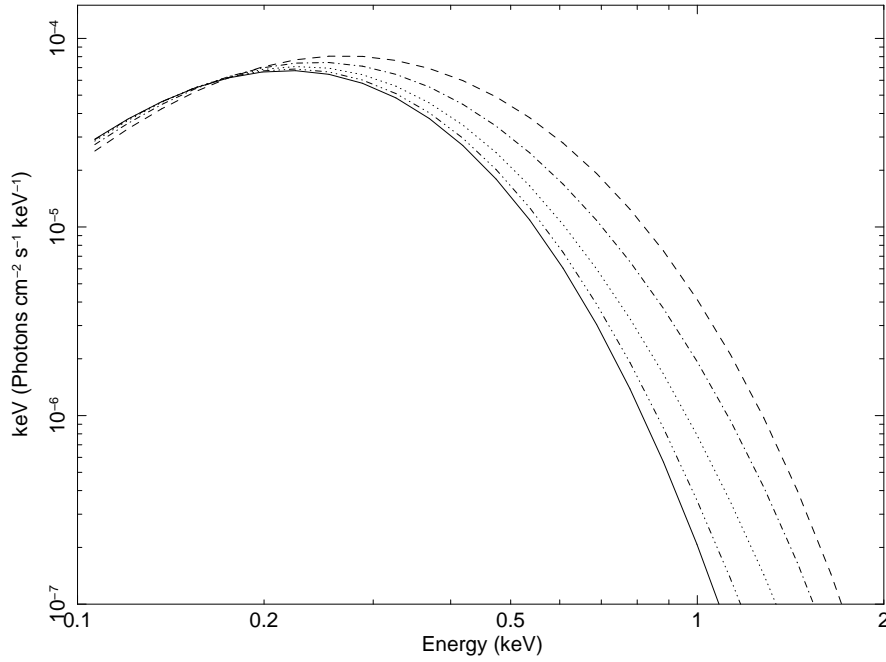


Fig. 4.— The spectral shapes with different q , in which the dash, dash dot, dotted and solid lines correspond to $q = 1, 2, 3, 4, 5$, and $kT_0 = 0.05 \text{ keV}, \beta_1 = 0.02, \beta_2 = 0.196$

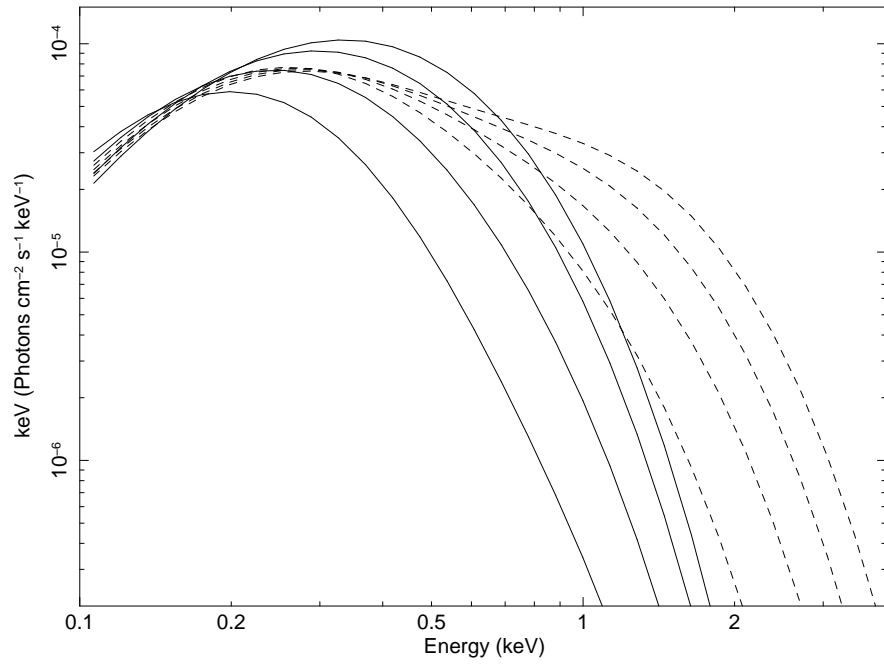


Fig. 5.— The spectral shapes with different β_1 and β_2 . Solid lines from down to up (above 0.5keV) correspond to $\beta_1 = 0.002, 0.020, 0.059, 0.098$ when $\beta_2 = 0.196$. Dotted lines from down to up (above 0.5keV) correspond to $\beta_2 = 0.391, 0.587, 0.783, 1$ when $\beta_1 = 0.02$. $kT_0 = 0.05\text{keV}$ and $q = 2$ are used.

Source	z	$\log M/M_{\odot}$	L/L_{Edd}	Observation ID
PG 0003+199	0.025	7.07	0.62	0306870101
PG 0844+349	0.064	7.66	0.41	0554710101
PG 0947+396	0.206	8.46	0.14	0111290101
PG 0953+414	0.239	8.52	0.58	0111290201
PG 1048+342	0.167	8.14	0.25	0109080701
PG 1116+215	0.177	8.41	0.74	0111290401
PG 1202+281	0.165	8.37	0.11	0109080101
PG 1211+143	0.080	7.81	1.14	0112610101
PG 1244+026	0.048	6.24	3.97	0051760101
PG 1307+085	0.155	8.50	0.24	0110950401
PG 1309+355	0.184	8.20	0.33	0109080201
PG 1322+659	0.168	7.74	0.81	0109080301
PG 1352+183	0.158	8.20	0.29	0109080401
PG 1402+261	0.164	7.76	1.24	0109081001
PG 1427+480	0.221	7.86	0.57	0109080901
PG 1440+356	0.077	7.28	1.07	0107660201
PG 1444+407	0.267	8.17	0.71	0109080601
PG 1501+106	0.036	8.23	0.12	0070740301
NGC 4051	0.002	6.13	0.31	0157560101
MRK 1044	0.016	6.23	1.25	0112600301
MRK 0359	0.017	6.23	1.79	0112600601
RE J1034+396	0.042	6.45	0.28	0561580201
PKS 0558-504	0.137	7.65	1.72	0125110101
MRK 0586	0.155	7.86	3.37	0048740101
TON S180	0.062	7.06	2.98	0110890401

Table 1: Source properties of AGNs analyzed. Mass and luminosity are taken from Middleton et al. (2007)

source	n_H	kT_0	β_1	β_2	q	Γ	reduced χ^2 (d.o.f.)
PG0003+199	2.83	0.07	0.053	0.770	3.60	1.92	1.294(973)
PG0844+349	2.32	0.05	0.063	0.571	3.35	0.97	0.995(297)
PG0947+396	2.22	0.03	0.028	1	3.14	1.97	0.946(866)
PG0953+414	0.90	0.01	0.066	1	1.01	2.32	0.966(871)
PG1048+342	1.20	0.08	0.002	0.461	1.82	1.68	0.927(412)
PG1116+215	1.78	0.04	0.027	1	3.25	2.31	0.951(928)
PG1202+281	1.03	0.04	0.074	1	3.68	1.65	1.003(598)
PG1211+143	3.26	0.02	0.007	1	2.85	2.06	1.164(1028)
PG1244+026	7.68	0.04	0.098	0.493	1.00	2.42	1.234(208)
PG1307+085	10.51	0.01	0.046	0.561	4.11	1.72	1.545(230)
PG1309+355	3.63	0.01	0.026	0.767	2.12	1.75	1.147(284)
PG1322+695	1.36	0.04	0.025	0.489	2.58	2.15	1.058(450)
PG1352+183	2.08	0.04	0.016	0.622	2.64	2.02	1.104(435)
PG1402+261	0.25	0.04	0.047	1	3.27	2.12	0.972(667)
PG1427+480	3.91	0.01	0.045	1	4.25	2.24	1.270(494)
PG1440+356	3.46	0.04	0.080	0.366	1.56	2.46	1.006(680)
PG1444+407	2.07	0.03	0.006	0.678	2.70	2.31	1.122(297)
PG1501+106	1.16	0.05	0.055	1	3.54	1.80	0.974(818)
NGC4051	1.04	0.10	0.035	0.362	2.95	1.25	2.051(1121)
Mrk1044	3.44	0.08	0.062	0.196	5.00	2.02	1.387(185)
Mrk0359	7.66	0.04	0.031	0.608	2.79	1.92	1.004(877)
REJ1034+396	4.90	0.04	0.098	0.290	1.42	2.50	1.196(746)
PKS0558-504	3.60	0.04	0.027	0.608	2.92	2.25	1.108(712)
Mrk0586	6.89	0.04	0.090	0.312	1.09	2.35	1.212(776)
TON S180	4.09	0.04	0.077	0.418	1.57	2.39	1.272(685)

Table 2: The fitting results of the sources. Γ is the hard X-ray spectrum index, kT_0 is the temperature of inner stable radius of accretion disk, in which n_H is in unit of 10^{20}cm^{-2} and kT_0 is in unit of keV .

source	$L_{soft}(\times 10^{44})$	ξ	$ratio(\%)$
PG0003+199 ^a	0.55	13.00	4.34
PG0844+349 ^b	3.78	4.13	10.90
PG0947+396 ^b	2.55	6.14	27.50
PG0953+414 ^b	7.77	2.96	8.69
PG1048+342 ^b	1.07	48.27	6.03
PG1116+215 ^b	5.00	3.87	6.21
PG1202+281 ^b	2.22	6.65	33.89
PG1211+143 ^b	0.16	19.00	0.82
PG1244+026 ^b	0.36	15.04	0.66
PG1307+085 ^b	0.36	5.33	3.39
PG1309+355 ^b	0.46	6.33	2.30
PG1322+695 ^b	2.21	6.00	4.80
PG1352+183 ^b	1.85	7.32	12.36
PG1402+261 ^b	2.70	5.25	3.30
PG1427+480 ^b	2.00	2.22	1.93
PG1440+356 ^b	1.00	9.35	3.02
PG1444+407 ^b	2.60	4.96	4.71
PG1501+106 ^b	0.57	20.07	26.71
NGC4051 ^a	0.015	146.80	2.82
Mrk1044 ^a	0.16	120.84	7.69
Mrk0359 ^c	0.07	46.08	0.86
REJ1034+396	-	-	-
PKS0558-504 ^d	68.1	0.59	4.24
Mrk0586 ^c	3.55	4.43	1.29
TON S180 ^a	68.1	0.53	2.46

Table 3: The estimated parameters by the model. L_{soft} is the observed luminosity. a: luminosity are taken from Grupe et al. (2010), b: luminosity are taken from Piconcelli et al. (2005), c: luminosity are taken from NED(<http://ned.ipac.caltech.edu/>), d: luminosity are taken from Mahony et al. (2010), and $ratio$ is the magnetic energy conversion rate.

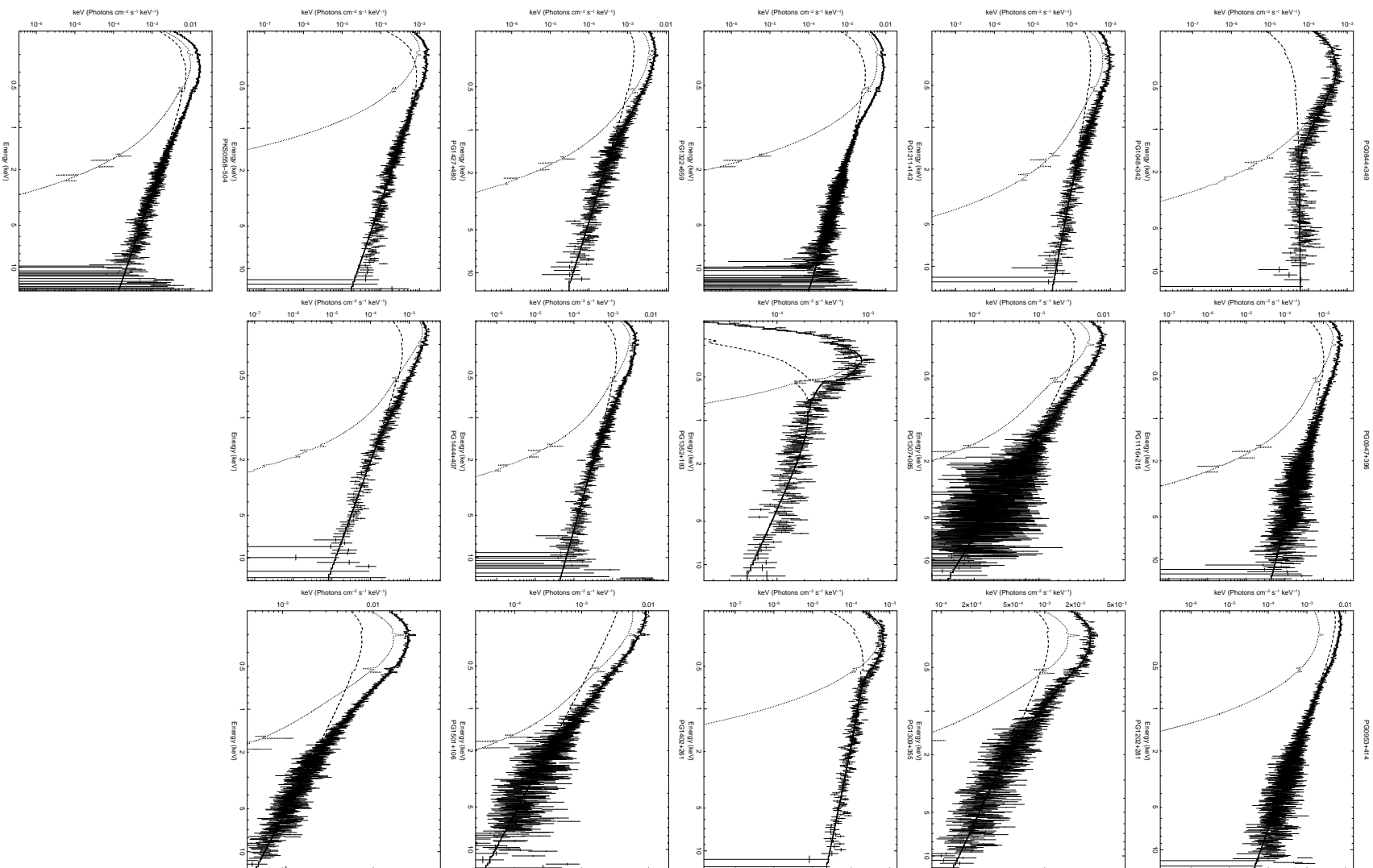


Fig. 6.— The fitting spectra. The black crosses are the data points, the solid line is the best fit to data. The dot line shows the inverse Compton scattering component from disc, and the dash line is the power law component from corona.

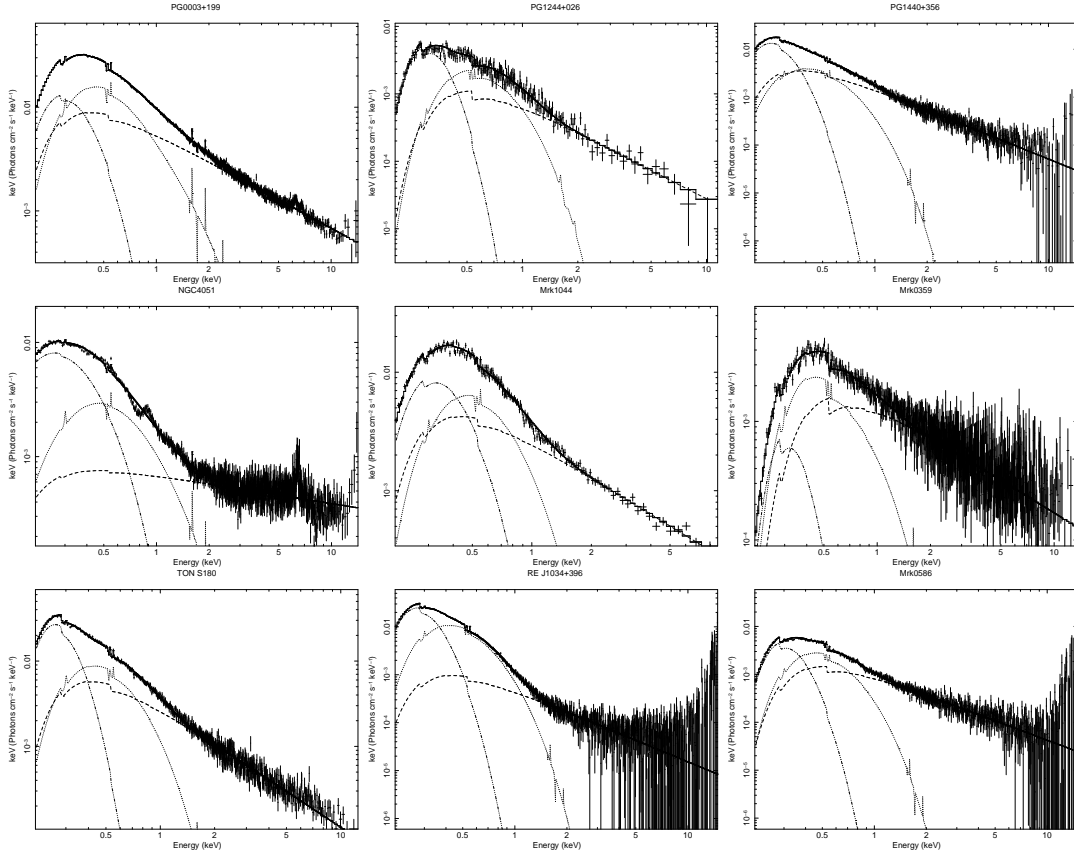


Fig. 7.— The fitting spectra with blackbody component. The black crosses are the data points, the solid line is the best fit to data. The dot and dash-dot lines show the inverse Compton scattering component and blackbody component from disc respectively. The dash line is the power law component from corona.